PNAS RESEARCH ARTICLE | APPLIED PHYSICAL SCIENCES OPEN ACCESS

Passage of exogeneous fine particles from the lung into the brain in humans and animals

Yu Qi[a,b], Shuting Wei[a], Tao Xin[c], Chuanjiang Huang[c], Yichen Pu[d], Jinzhu Ma[a,b], Changbin Zhang[a,b], Yajun Liu[e,f], Iseult Lynch[g], and Sijin Liu[a,b,f,1]

Edited by Catherine Murphy, University of Illinois at Urbana–Champaign, Urbana, IL; received September 16, 2021; accepted May 17, 2022

There are still significant knowledge gaps in understanding the intrusion and retention of exogeneous particles into the central nervous system (CNS). Here, we uncovered various exogeneous fine particles in human cerebrospinal fluids (CSFs) and identified the ambient environmental or occupational exposure sources of these particles, including commonly found particles (e.g., Fe- and Ca-containing ones) and other compositions that have not been reported previously (such as malayaite and anatase TiO_2), by mapping their chemical and structural fingerprints. Furthermore, using mouse and in vitro models, we unveiled a possible translocation pathway of various inhaled fine particles from the lung to the brain through blood circulation (via dedicated biodistribution and mechanistic studies). Importantly, with the aid of isotope labeling, we obtained the retention kinetics of inhaled fine particles in mice, indicating a much slower clearance rate of localized exogenous particles from the brain than from other main metabolic organs. Collectively, our results provide a piece of evidence on the intrusion of exogeneous particles into the CNS and support the association between the inhalation of exogenous particles and their transport into the brain tissues. This work thus provides additional insights for the continued investigation of the adverse effects of air pollution on the brain.

air pollution | particulate matters | ambient exposure | brain health | particle retention

Significance

Addressing the knowledge gaps regarding the access to and harmful effects of airborne fine particles on the central nervous system is critical. Various exogenous fine particles were found in human cerebrospinal fluids, including commonly found particles and others that have not been reported previously. Animal experiments provided mechanistic explanations and verifications of the translocation of inhaled particles into the brain. Moreover, retention of particles in the brain for longer durations than in other organs was demonstrated through isotope labeling–based biodistribution studies in mice, suggesting possible long-term effects on the brain. This work unravels indications and associations between inhalation and particle transport and adds evidence on the relationship between air pollution and detrimental effects of exogenous particles on the brain.

Air pollution is still a great threat to public health globally. In the past decades, the lung and cardiovascular systems have been considered the predominant organs afflicted by air pollution as evidenced by numerous epidemiological and experimental findings (1–3). Meanwhile, recent evidence recognizes the likely injuries in the brain arising from extended exposure to polluted air and the consequent neurodegenerative diseases and behavioral disorder symptoms (4, 5). For instance, observations revealed a strong link between high levels of air pollution and marked neuroinflammation, Alzheimer's-like changes, and cognitive problems in older people and even in children (6–12). Maher et al. (13) observed the presence of magnetic particles with a size less than 200 nm in the human frontal cortex and proposed the entry of particles into the brain via the olfactory bulb. More recently, Calderón-Garcidueñas et al. (14) identified the existence of exogenous metal-rich and magnetic fine particles and Ti-rich nanorods in the human brain and also showed evidence of entry via axonal transport, namely from the gastrointestinal tract, as the key entry portal and subsequent transport to the brain stem via the vagus nerves. In support of these findings in humans, experimental studies obtained similar observations in different animal models (15–18). However, much less is understood regarding the impact of ambient fine particles on the brain compared with their impact on the lung and heart. For instance, there is a lack of evidence on the intrusion of exogeneous fine particles from environmental or occupational sources into the brain as well as a lack of evidence regarding the exposure route and transport process of exogeneous particles, particle-induced injuries to the surrounding brain tissue, and the accumulation and retention kinetics of particles in the brain. To understand the scale of the issue, it would be of great significance to fill these knowledge gaps on airborne fine particles and their impacts on the brain.

Air pollutants are a mixture of many toxic components. Of various pollutants, particulate matters (PMs), especially ambient fine particles (such as $PM_{2.5}$ and $PM_{0.1}$), are thought to be the most concerning in terms of their induction of detrimental health effects (19). Many physicochemical properties have been documented to dictate the toxicity of PMs, and the ambient particle size appears to be the most decisive one (20). Hence, PMs, in particular ultrafine particles, bear an intrinsic capability to escape the recent monitoring techniques and the body's protective systems, including the sentinel immune cells and the biological barriers (21–24). In fact, inhaled ambient fine particles or exogeneous engineered nanoparticles (NPs) have been observed in human serum

Author contributions: Y.Q., J.M., C.Z., Y.L., and S.L. designed research; Y.Q., S.W., T.X., C.H., and Y.P. performed research; Y.Q. analyzed data; and Y.Q., S.W., T.X., C.H., Y.P., J.M., C.Z., Y.L., I.L., and S.L. wrote the paper.

The authors declare no competing interest.

This article is a PNAS Direct Submission.

[1]To whom correspondence may be addressed. Email: sjliu@rcees.ac.cn.

This article contains supporting information online at http://www.pnas.org/lookup/suppl/doi:10.1073/pnas.2117083119/-/DCSupplemental.

Published June 22, 2022.

(25), pleural effusion (25), heart tissue (26), vascular inflammation (27), and even the placenta (28). Unlike the liver, spleen, and other organs with defenseless large-volume blood circulation, the brain is naturally protected by a stringent defense line, namely the blood–brain barrier (BBB), which prevents the crossing of both soluble and particulate foreign entities or offenders (29, 30). Under this premise, it is rather difficult for PMs to penetrate the BBB; however, crossing may occur when the integrity of the BBB is impaired or if the PMs per se damage the BBB (5, 30). To date, multiple pathways have been proposed for the direct intrusion of PMs into the brain (4, 5, 31). One pathway bypasses the BBB, typically through the nose–olfactory route, and this has been confirmed for some synthesized (engineered) NPs (21, 22, 31, 32). The second pathway is in the capacity of nanoscale particles to bind specific proteins, such as apolipoprotein E from plasma, which interact with cellular receptors in the BBB and thus, actively aid the transportation of the particles into the brain via transcytosis without damaging the BBB (33, 34). Meanwhile, the third pathway (i.e., through the inhalation–circulation–BBB route) relies on damage of the BBB, but it is still under debate (4, 5). Moreover, an additional pathway (i.e., the neuroenteric pathway) was indicated to translocate fine particles to the brain from the digestive system, as it is through the neurons of the enteric system to the brain (stem) (14). Since significant BBB impairments were found in animals responding to heavy PM exposure (15, 16), whether the inhaled atmospheric PMs could translocate from blood to the brain ventricle through damage to the BBB needs to be elucidated. To this end, these passive and active pathways for PMs through the BBB warrant detailed investigations.

In the current study, we aimed to investigate the intrusion and retention of exogenous fine particles into the brain using in vitro and in vivo models with the aid of ultrastructural microscopy and isotope-labeled particles and to use this knowledge to scrutinize the retention of exogeneous particles in human brain tissues from hospitalized patient samples. Collectively, our combined results revealed the presence of exogeneous fine particles of various compositions in human cerebrospinal fluid (CSF) and added experimental proof (in vivo in mice and in vitro) for the transport of inhaled fine particles into the brain. This work provides further evidence for a potential pathway by which air pollution may exert effects on the brain.

Results

Identification of Exogenous Fine Particles in Human CSF and Blood. In order to determine whether exogeneous fine particles can accumulate in the human brain, we collected and characterized human CSF and blood specimens from patients who experienced brain diseases but had not received any previous brain surgery. CSF is generated by the choroid plexus in each ventricle of the brain and is responsible for protecting the brain against mechanical shock (29). It circulates among the whole brain, including the ventricles, arachnoid, and aqueduct, and is involved in the removal of the secreted exhausts and exogeneous components from the brain (29). Therefore, the presence of exogeneous components in CSF is indicative of metabolites from the central nervous system (CNS) or foreign invaders (e.g., particles) that have reached into the ventricles through the BBB (29, 35–38).

Hereby, we uncovered exogeneous fine particles in 8 of 25 different CSF specimens from 25 patients (32% of the total specimens evaluated) (*SI Appendix*, Table S1) as identified by high-resolution transmission electron microscopy (HR-TEM) and high-angle annular dark field scanning transmission electron microscopy (HAADF-STEM) combined with energy-dispersive X-ray spectroscopy (EDXS). Overall, the exogeneous fine particles identified in the eight CSF samples varied in composition, but some had elemental components commonly found in the atmospheric environment, including calcium (Ca), silicon (Si), and iron (Fe). In more detail, the exogeneous particles identified in the first and second patients' CSF specimens are both $CaCO_3$ but with differential structural fingerprints, referring to calcite and aragonite, respectively (*SI Appendix*, Figs. S1 and S2 and Table S1, samples 1 and 2 exogeneous particles). Calcium-based minerals are frequently used as raw material in construction and also as an abrasive, agricultural soil treatment, pigment, pharmaceutical additive, and others in diverse applications (39). Fe-containing and Si-containing particles were also found in the CSF specimens, such as $CaFe_2O_4$ and SiO_2 (*SI Appendix*, Figs. S3–S6 and Table S1, samples 3 to 6 exogeneous particles), consistent with previous studies (14, 25, 40–42). Humans are likely to be exposed to Fe- and Si-containing particles environmentally, and for example, such Fe-containing particles were also observed in human brain (13, 14), heart (26), blood (25), pleural effusion (25), and knee joint effusion (as recently reported by our group) (43).

In addition to these commonly found exogeneous fine particles, we also recognized distinct types of particles in humans that have not been reported in human exposure previously. Figs. 1 and 2 show representative exogeneous fine particles observed in the CSF specimens. The first one (*SI Appendix*, Table S1, sample 7 exogeneous particle) appeared as an aggregate with an amorphous morphology and a diameter of around 50 nm (Fig. 1*A*). The second one (*SI Appendix*, Table S1, sample 8 exogeneous particle) also appeared as an aggregate but was composed of three sphere-like particles, and the size of each particle was ∼80 to 100 nm (Fig. 2*A*). Further, the detailed fingerprint information, including elementary compositions, structure, and crystal lattice indexing, unveiled that the first one consisted of malayaite ($CaSnSiO_5$; powder diffraction file [PDF] 25-0176) (Fig. 1 *C–I*), which is widely used as a pigment in the ceramic industry for coloring glazes (44). Interestingly, the second one showed Ti and O as the main components as shown by EDXS (Fig. 2*B*). HAADF-STEM demonstrated the presence of (200), (215), (116), and (220) facets (Fig. 2 *C–H*), being ascribed to anatase TiO_2 (PDF 21-1272), which is widely used in sunscreens and as a pigment in paints and coatings (45). The presence of malayaite fine particles in human tissue or CSF has not been reported previously. Malayaite is a type of monoclinic–prismatic mineral that occurs in the natural environment, and it is usually used in ceramic paints, especially in China, and/or building materials together with titanite (44, 46, 47). Intriguingly, the patient whose CSF was found to contain ceramic-derived particles (i.e., malayaite) is a worker in traditional Chinese folk handicrafts and handles diverse types of paints daily. Thus, exposure in this case could be either environmental or occupational, and it is more likely the latter. Meanwhile, the entry of TiO_2 into human tissues/organs upon inhalation exposure (e.g. , the brain stem, neuroenteric tissue, pleural effusion, and serum) has been demonstrated in previous studies (14, 25), as nano-TiO_2 is widely applied in catalysts, paint and building adducts, food, daily consumer products, and personal care products (45, 48). Thus, human exposure to TiO_2 NPs might be via multiple routes, such as skin, food ingestion, drinking, and inhalation (48, 49). Notably, the anatase phase of TiO_2 found here is a naturally occurring mineral, while the rutile phase of TiO_2 is often produced in a high-temperature environment, such as during calcination (45). This is a report on the human exposure of anatase

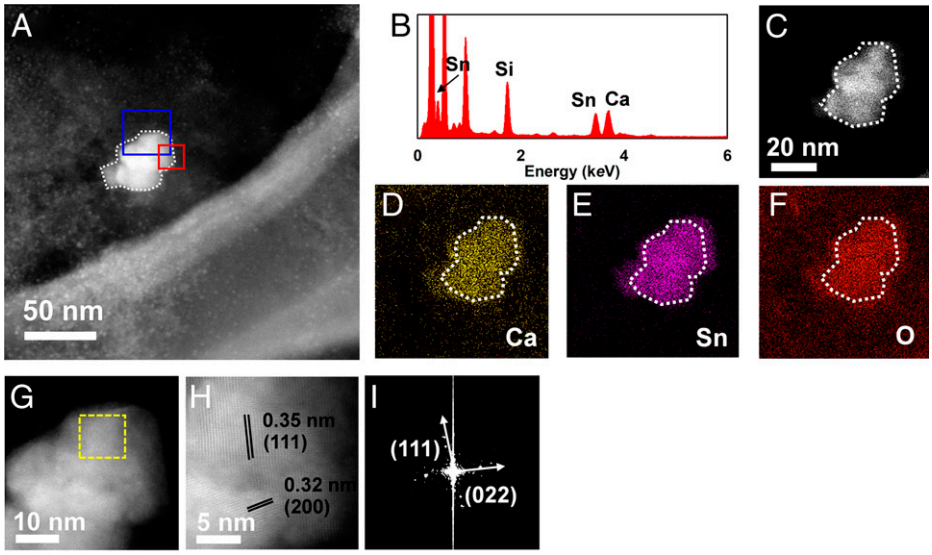

Fig. 1. Structural and chemical fingerprints of representative exogenous fine particles observed in a human CSF specimen. (*A*) HAADF-STEM image of a particle aggregate extracted from a CSF specimen from a patient who suffered from cerebral hemorrhage. (*B*) The EDXS spectrum indicates pronounced signals from the elements Sn, Si, and Ca. The EDXS mapping of the particle aggregate (*C*–*F*) further confirms the elemental composition, corresponding to the EDXS spectrum. A high-resolution HAADF-STEM image (*G*) of the blue square marked in *A* and an atomic-resolution HAADF-STEM image (*H*) of the red square marked in *A* show the crystalline facets of (111) and (200) as indicated by the parallel sets of black lines. (*I*) The fast Fourier transform of the area in *G* labeled with a yellow square also substantiates the crystalline facets of (111) and (022). The structural and chemical fingerprints of the particles consistently refer to the mineral malayaite ($CaSnSiO_5$; PDF 25-0176).

TiO_2, and it more likely came from environmental exposure rather than occupational exposure. These results collectively suggested that various exogenous fine particles can enter the human brain and can be excreted as intact and agglomerated particles into the CSF.

It should be noted that only a small proportion of the whole CSF volume was examined here, and thus, at present, it is rather difficult to precisely quantify the total number of particles in the brains of these patients due to limitations in sampling. Encouragingly, Calderón-Garcidueñas et al. (14) recently estimated the concentrations and numbers of magnetite-like NPs in human brains from residents of Mexico City, signifying a large variation in the number of NPs in the brain. Therefore, we also attempted to roughly estimate the particle numbers in human CSF specimens based on the HR-TEM analysis. For example, more than ten thousands of particles were estimated in the whole CSF of patient #5. Also, since CSF is the circulating medium among ventricles, there may be massive numbers of particles taken up (endocytosed and phagocytosed) by the diverse cells in the brain tissue and thereafter localized therein, which means that the actual number of particles in the brain should be higher than we estimated for CSF. A detailed description of the deduction and number estimation is in *SI Appendix*, *SI Text* and Table S1. Although the current data on CSF differed in the

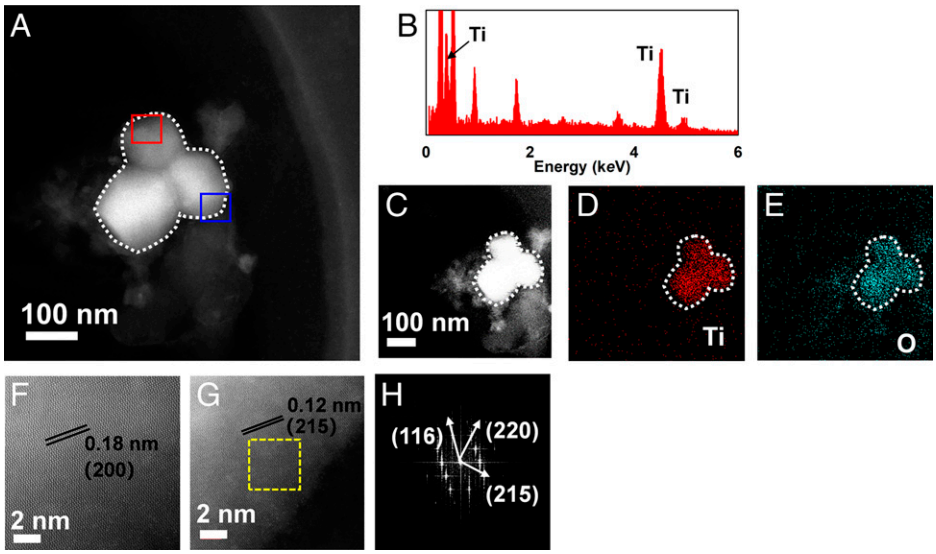

Fig. 2. Morphological and chemical fingerprints of representative exogenous fine particles in a human CSF sample. (*A*) Morphology of the particle aggregate with a size around 200 nm (appearing as three spherical particles; ~80 to 100 nm in diameter for each) extracted from a CSF specimen from a patient with neuroinflammation as characterized by HAADF-STEM imaging. (*B*) The EDXS determination of the particles denotes abundant signals of the Ti element. The EDXS mapping of the particles (*C*–*E*) shows the elemental composition corresponding to the EDXS spectrum (Ti and O). Atomic-resolution HAADF-STEM images of the red square (*F*) marked in *A* and the blue square (*G*) marked in *A* reveal the crystalline facets of (200) and (215), respectively, indicated by the parallel black lines. The fast Fourier transform image (*H*) representative of the yellow square marked in *G* corroborates the facets (116), (220), and (215). Based on all these determinations, the particles are confirmed to be anatase TiO_2 (TiO_2; PDF 21-1272).

order of magnitude for the particle numbers due to great discrepancies in specimens, sources, and methodologies in comparison with previously published data on brain tissue (14), our findings together with previous findings strikingly unraveled the exposure of significant mass and diverse types of exogenous particles in the human brain rather than only the argument over the presence vs. absence of exogenous particles. Nevertheless, the low number of patients and the fact that CSF is not generally available mean that extrapolation to the general population is challenging, but the findings here likely reflect the occurrence of substantive numbers of exogeneous fine particles in human CSF in some patients, mostly from occupational exposures, and warrant follow-up epidemiological studies and wider utilization of CSF biobanks for example (50). Thus, the identification of various types of exogenous fine particles with noticeable mass in CSF is significant, showing a potential link between air pollution particles and brain effects.

There are several ways through which exogenous particles may enter the brain. Particles that pass through the olfactory bulb or through the cellular receptor system do not need to damage the BBB, a tight barrier comprising endothelial cells that prevents unnecessary substances from crossing into the CNS. In the lung to brain route, particles must circulate through the bloodstream, and they likely acquire a layer of absorbed proteins and other biomolecules, which is referred to as corona formation, as previous studies found for engineered NPs (27, 51–53) and may cross from the bloodstream through the BBB without visibly damaging it for final localization in the ventricles of the brain (30). In line with this route, we further found exogenous particles, including malayaite and SiO_2, in blood specimens from the patients (Fig. 3 and *SI Appendix*, Fig. S7 and Table S2). As shown in Fig. 3, malayaite particles with the same morphological and structural fingerprints ($CaSnSiO_5$; PDF 25-0176) were found in the blood sample as identified by HAADF-STEM and EDXS, indicating that the entry of exogenous particles into the brain from the bloodstream is highly possible, although whether this is realized via receptor-mediated transportation or through damage to the BBB is not clear yet. Notably, it would be impossible for the larger fine particles found in CSFs, such as those around 400 nm (*SI Appendix*, Fig. S4), to gain access via the olfactory bulb as demonstrated previously (13, 14), signifying the route of the large-sized inhaled fine particles via the bloodstream and finally, into the brain. Building on previous reports of exogeneous particles found in the human body, our results appear to extend the possible exposure scenarios, especially from the ambient environment, as supported by the findings of the typical ambient particles from paints and catalysts and to extend the range of exogenous particles found in human specimens in recent studies (14, 25, 54, 55). For comparison, exogeneous particles were carefully examined in blood specimens from 26 healthy control individuals. Only one suspected exogeneous particle aggregate was found in a blood sample. Since all our human CSF specimens came from hospitalized patients with brain disorders, our results may imply an important relationship between exogenous particle-induced neurotoxicity and brain disorders as previous studies suggested (6, 13, 14).

Experimental Validation of Exogenous Fine Particle Intrusion into the Brain from Inhalation in Animals. To demonstrate the possibility of ambient fine particle entry into the brain, we conducted animal experiments that mimicked the inhalation exposure route. To exclude the unwanted exposure pathway through the nasal cavity (namely the olfactory bulb pathway), mice were directly administrated exogenous particles by intratracheal instillation. To better imitate the exogenous particles discovered in the human brain as described above, we used small-sized TiO_2 particles (TiO_2 nanoparticles, Degussa P25 with a size of 10 to 30 nm) (*SI Appendix*, Fig. S8), which are commonly found in the atmospheric environment (48, 49, 56), as a representative of mineral particles. We also used carbon black (CB) particles (30 to 50 nm) (*SI Appendix*, Fig. S9) as a representative of airborne anthropogenic particles, as CB is the core of airborne PMs (28).

The BALB/c mice (females, 6 to 7 wk old, 20 g average body weight) were administered with P25 or CB intratracheally at 2.5 mg/kg body weight to simulate accumulated inhaled PM exposure as previously described (57–61). The exposure did not induce overt pathological changes in the heart, liver, lung,

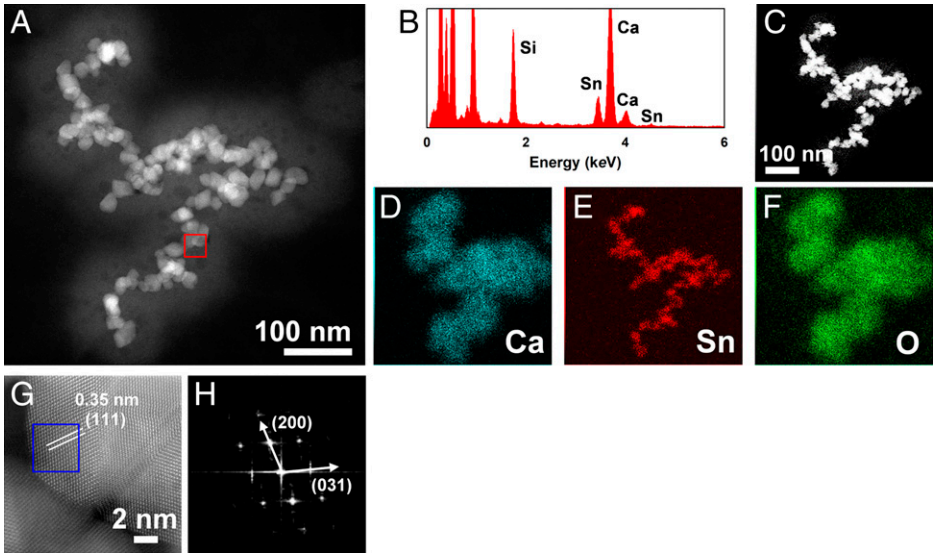

Fig. 3. Structural and chemical fingerprints of representative exogenous fine particles in a human blood sample. (*A*) HAADF-STEM imaging of the particles extracted from a human blood specimen from a patient with cerebral hemorrhage shows aggregates of multiple amorphous spherical particles. (*B*) The EDXS spectrum of the particles indicates ample signals of Sn, Si, and Ca, consistent with the particles found in the CSF specimen, as described in Fig. 1. The EDXS mapping of these particles (*C*–*F*) confirms the element compositions. The atomic-resolution HAADF-STEM image of the red square marked in *A* shows the crystalline facet of (111), and the fast Fourier transform image (*H*) representative of the blue square marked in *G* corroborates the facets (200) and (031), respectively. These structural and chemical fingerprints confirm the particles as being malayaite ($CaSnSiO_5$; PDF 25-0176).

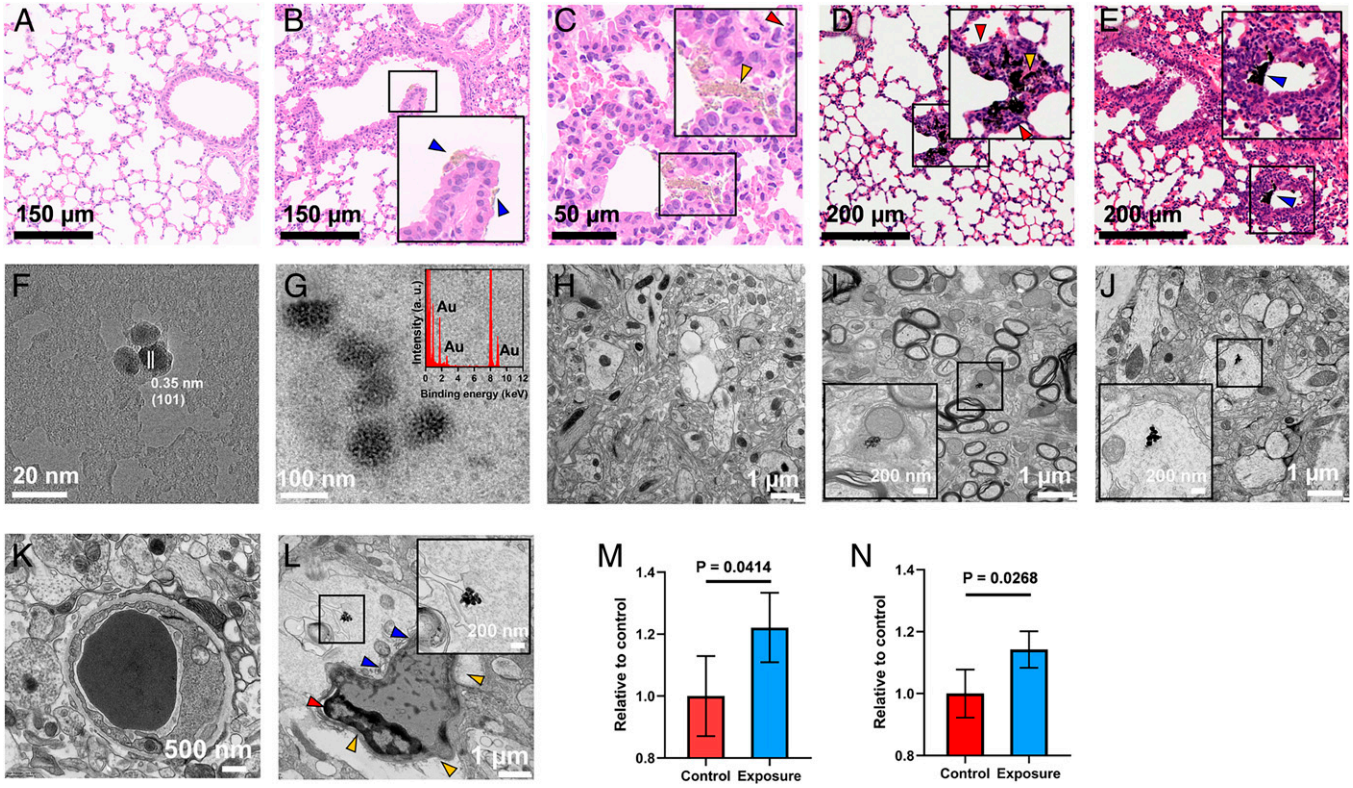

Fig. 4. Characterization of the uptake pathway of exogenous fine particles and particle accumulation in tissues using a mouse model. (*A*–*E*) Hematoxylin and eosin staining of the lung tissues from the untreated control group (*A*), the TiO_2 exposure group (*B* and *C*), and the CB exposure group (*D* and *E*), with *Insets* showing enlarged views of the particle aggregates in the lung sections. The particle aggregates are denoted by blue arrowheads in the alveoli, infiltrated inflammatory cells are indicated by red arrowheads, and translocated particles from the alveoli into septa and capillaries are indicated by yellow arrowheads. The HR-TEM image displays the extracted TiO_2 particles (*F*) and Au-doped CB particles (*G*, with an *Inset* showing the EDXS spectrum) from mouse blood following translocation across the air–blood barrier. Compared with the untreated control (*H*), the HR-TEM images exhibit TiO_2 (*I*) and CB particles (*J*) in mouse brain tissues, with *Insets* showing enlarged views of particle aggregates in the brain sections. The ultrastructures of the blood vessels in the control group (*K*) and the CB exposure group (*L*, with an *Inset* showing enlarged view of the particle aggregate near the blood vessel) show different morphologies, as the control group exhibits a thin and uniform basement membrane, but the exposure group manifests structural damage with irregular and defective basal lamina (blue arrowheads), shrinking of endothelial cells (red arrowhead), and deformation of the vessel (yellow arrowheads). The quantification of EB extravasation contents is shown for TiO_2 (*M*) and CB (*N*) exposure groups ($n = 4$) relative to the untreated group. Data are presented as mean ± SD.

spleen, and kidney (*SI Appendix*, Figs. S10 and S11), suggesting that a mild sublethal exposure was achieved. Twenty-four hours postexposure, compared with untreated controls (Fig. 4*A*), marked particle aggregates (Fig. 4 *B*–*E*) could be visualized in the alveoli (Fig. 4 *B* and *E*, blue arrowheads). As a consequence, significant alveolar injury and inflammation, coupled to infiltration of inflammatory cells, were observed in mice upon exposure to P25 and CB relative to untreated controls (Fig. 4 *C* and *D*, red arrowheads). Moreover, pronounced transmission of P25 and CB particles across the air–blood barrier could be defined as evidenced by the marked translocation of particles from the alveoli into septa and capillaries (Fig. 4 *C* and *D*, yellow arrowheads), revealing the translocation of particles into blood circulation from which they can reach the far sites of the body.

The entry of the particles into the bloodstream by crossing the air–blood barrier was then demonstrated by the observation of the particles in blood samples using HR-TEM (Fig. 4 *F* and *G*). Particles with sizes of 20 nm were observed in the blood of P25-exposed mice (Fig. 4*F*). HR-TEM revealed the (101) crystalline facet, in analogy to the pristine TiO_2 that was used for the exposure experiment (*SI Appendix*, Fig. S8). Unlike TiO_2, which can be easily separated from biological medium, recognition of CB against the carbon background in biological samples is difficult. Thus, a labeling strategy was performed using gold (Au) as an enabling tracer following a previously described method (62), allowing the identification of CB through EDXS coupled with HR-TEM (*SI Appendix*, Fig. S12). The stability test revealed negligible Au ion release from doped Au on the particles in a biological medium, such as phosphate buffer saline (PBS; pH 7.0) (*SI Appendix*, Fig. S8*C*), and even in artificial lysosomal fluid (pH 4.5) (*SI Appendix*, Fig. S8*D*), demonstrating the considerable stability of the Au-doped CB particles in biological settings. For the CB treatment group, we used Au-doped CB to enable detection and quantification. As shown in Fig. 4*G*, particles with a size of 50 nm were observed in the blood. A strong Au signal was detected by EDXS, confirming that the particles were Au-doped CB. These results thereby revealed that the exogeneous particles circulated through the bloodstream after crossing the air–blood barrier.

Next, we examined whether the particles in the bloodstream corresponded to those transported to the brain. To strengthen our work, we here added three more particle types (i.e., Au, CeO_2, and quantum dot [QD] NPs) with similar size and morphology to CB and P25 (*SI Appendix*, Fig. S13). Au, CeO_2, and QD NPs were also administered intratracheally at 2.5 mg/kg body weight. Compared with untreated control brains where there was no evidence of foreign particles (Fig. 4*H*), aggregates of P25 (Fig. 4*I*) and CB particles (Fig. 4*J*) were found in the brains of the exposed animals. P25 particles in the brain tissue were confirmed by EDXS-coupled environmental scanning electron microscopy (*SI Appendix*, Fig. S14). In more detail, particle aggregates were visualized in different regions of the brain, such as the cerebral cortex, hippocampus, and cerebellum (*SI Appendix*, Fig. S15 and Table S3). Notably, particle

aggregates that are much larger than the original particle size were observed in some subcellular structures within the brain cells, analogous to previously reported findings (14). The BBB region showed a well-organized vessel structure in the brain of mice with no particle treatments (Fig. 4*K*). In contrast to the blank control, we observed quite a few NP aggregates near the BBB in the brains of treated mice. For example, as shown in Fig. 4 *L*, *Inset*, a particle aggregate was found in the brain tissue near the BBB in the current field of the brain section from a treated mouse, suggesting the entry of particle aggregates into the brain. Strikingly, the BBB structure was damaged as evidenced by the deformation of the blood vessel and a partial loss of basal lamina and tight junctions around endothelial cells (denoted by arrowheads in Fig. 4*L*). Intriguingly, aggregates were found inside and outside the blood vessel near the BBB in several brain slices for these particles. For example, an Au particle aggregate was found in the blood vessel, and nearby particle aggregates outside the vessel were also observed (*SI Appendix*, Fig. S16). Moreover, the presence of aggregates in the blood vessels also revealed the transformation of exogenous particles into the aggregate form prior to transport into the brain rather than the transport of single particles and their aggregation following invasion into the brain. The cerebral vascular leakage was further verified by the Evans blue (EB) test, as ∼20% increased leakage of EB dye was seen in mice exposed to P25, CB, and other particles compared with the untreated groups (Fig. 4 *M* and *N* and *SI Appendix*, Fig. S17) ($P < 0.05$), indicative of BBB damage.

To elucidate the mechanisms underlying the particle translocation through the BBB, we established an in vitro model dependent on the coculture of mouse brain–derived endothelial (bEnd.3) cells with mouse primary astrocytes (*SI Appendix*, Fig. S18*A*) as previously established (30, 63). A robust induction of zonula occludens-1 (ZO-1) indicated the successful setup of the in vitro BBB model, and the decrease of the ZO-1 level after particle treatment implied damage of the tight junctions (*SI Appendix*, Fig. S18*B*), analogous to previous reports (30). After exposure to particles, the medium in the basolateral chamber was collected for HR-TEM observation and inductively coupled plasma mass spectrometry (ICP-MS) analysis to quantify the particle transport. As shown in *SI Appendix*, Fig. S18 *C–H*, particles were visualized in the basolateral chamber, confirming the translocation of particles through the BBB. This observation was further substantiated by the analysis by ICP-MS (*SI Appendix*, Fig. S18*I*). It should be noted that the migrated particles appeared as both aggregates and single particles in the basolateral chamber, indicating passage of both forms through the in vitro BBB model, in analogy to the current understandings (30). Together, in support of our animal experiments, the in vitro BBB experiments uncovered the translocation from the apical chamber to the basolateral chamber through the in vitro BBB for CB, TiO_2, Au NPs, CeO_2 NPs, and QDs. As an extension of previous findings (4, 20, 22, 31, 32, 54), our in vitro and in vivo findings supported the transport process of particle intrusion into the brain namely from the lung via blood to the brain, eventually leading to potential long-term detrimental effects on the brain.

Particokinetics of Exogenous Particles in the Brain and Other Organs. Determining the retention kinetics of exogenous particles in the brain together with other main organs can help us to understand their long-term toxicity and their primary and secondary translocation among organs. We therefore examined the retention kinetics of CB particles as an ideal representative of realistic airborne PMs using the ^{125}I isotope–labeling method. As shown in *SI Appendix*, Fig. S19, the CB particles were stably labeled with ^{125}I as established previously (64). Our labeled particles showed great stability in various biological media at least for 15 d (*SI Appendix*, Fig. S19). The ^{125}I-labeled CB particles were also administered intratracheally at 2.5 mg/kg body weight. With the detection of the ^{125}I isotope signal, we could readily determine the particokinetics of CB particles in the brain, blood, heart, spleen, liver, kidney, and lung (*SI Appendix*, Fig. S20). The CB particles accumulated rapidly in different organs, including blood, liver, spleen, kidney, and lung (*SI Appendix*, Fig. S20), indicating the retention of foreign particles by reticuloendothelial cells in these organs as previously discussed in the literature (2, 65). The high signal detected in the kidney suggested that the predominant clearance route of exogenous particles is through renal excretion, in agreement with previous findings on other nano-sized particles (64, 65). Accumulation of CB in the brain reached 1.25 (the percentage of the injected dose per gram of tissue, ID/g × 10^{-2}%) in 24 h and dropped to 0.13 (ID/g × 10^{-2}%) after 15 d (*SI Appendix*, Fig. S20). Noteworthily, the signal from labeled particles was also strong in the brain on day 1, corroborating the invasion of exogenous particles into the brain. For comparison, the same dose of $Na^{125}I$ was exposed to mice through intratracheal instillation. In the $Na^{125}I$ group, free ^{125}I anions were quickly cleared from the body within 24 h through renal metabolism, and retention in the brain and other organs was negligible relative to that of labeled particles (*SI Appendix*, Table S4), suggesting distinct retention profiles of exogenous particles.

To further understand the particokinetics, the retained burden in different organs at different times was calculated as a percentage of the retention on day 1 after exposure. An exponential decline trend was observed in all organs over time (Fig. 5). Specifically, the accumulation of exogenous particles dramatically dropped in all places quickly after 1 d, as reflected by the decline of the ^{125}I isotope signal from day 3 to day 15 ($P < 0.001$) (Fig. 5 and *SI Appendix*, Fig. S20). The clearance of exogenous particles from the brain seemed to be slower and more difficult compared with clearance from other organs (Fig. 5*A* and *SI Appendix*, Fig. S16*A*). To further depict the particokinetics of exogenous particles, a one-phase decay model was applied to analyze the experimental data according to a published method (66), where the K values of different organs represent the clearance rate per day for a one-compartment model (Fig. 5*H*) (49, 66). Compared with other organs (i.e., the spleen, liver, and kidney), the brain revealed a much slower clearance rate (Fig. 5*A*). Specifically, the K values of the blood, heart, spleen, liver, kidney, and lung were 1.051, 0.480, 1.262, 0.791, 1.051, and 1.051, respectively, whereas the K value of the brain was 0.246. The half-life values ($t_{1/2}$) were calculated to be 0.660, 1.444, 1.262, 0.876, 0.660, and 0.660 d for blood, heart, spleen, liver, kidney, and lung, respectively, while in the brain, the exogenous particles showed a significantly longer half-life (2.822 d), indicating longer retention. Although the absolute amount of CB accumulation may not be comparable with other organs, the longer retention and difficulty in clearance of CB from the brain could potentially lead to neurotoxicity in the brain. These results clearly suggested that exogenous particles retained in the CNS could not be readily excreted due to the complex brain structure and anatomy (Fig. 6), especially the reverse barrier function by the BBB and its role in maintaining brain homeostasis, and the limitations in lymphatic drainage, implying more lasting toxic effects of exogenous particles on the brain tissues and surrounding cells (67, 68).

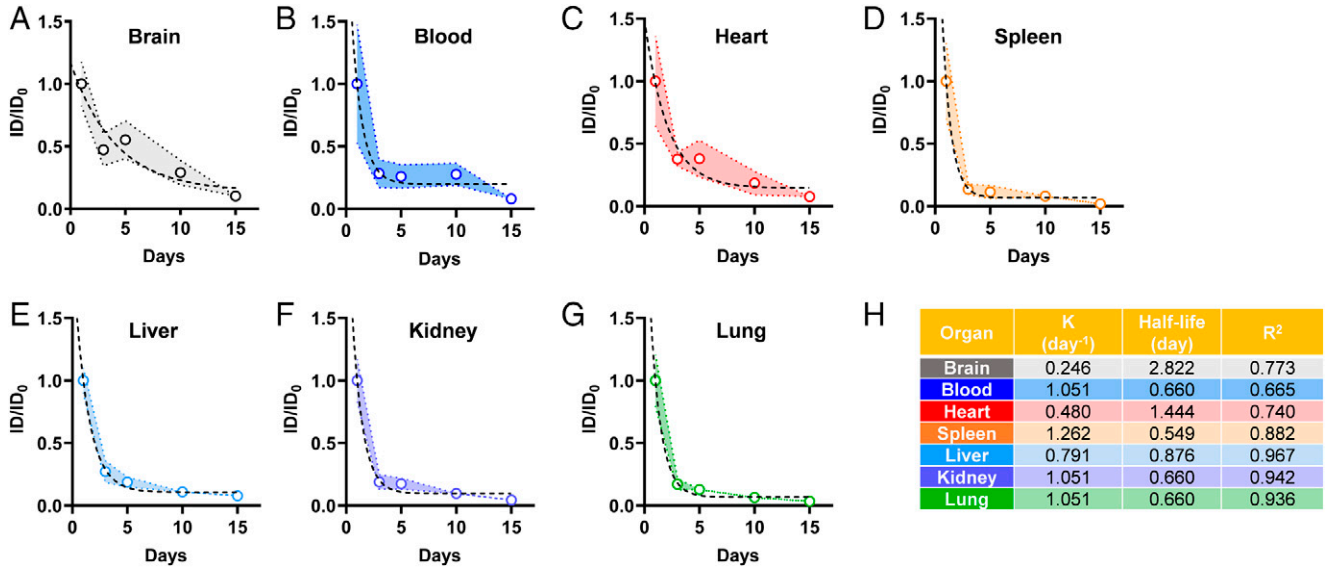

Organ	K (day^{-1})	Half-life (day)	R^2
Brain	0.246	2.822	0.773
Blood	1.051	0.660	0.665
Heart	0.480	1.444	0.740
Spleen	1.262	0.549	0.882
Liver	0.791	0.876	0.967
Kidney	1.051	0.660	0.942
Lung	1.051	0.660	0.936

Fig. 5. Retention kinetics of ^{125}I-labeled CB particles in mice at different time points up to 15 d after intratracheal instillation. The data were analyzed using the one-phase decay model for the brain (*A*), blood (*B*), heart (*C*), spleen (*D*), liver (*E*), kidney (*F*), and lung (*G*). Calculated data reveal the corresponding clearance rates ($n = 8$). The ID_0 represents the original injected dose. The calculated parameters for the rate constant (K), half-life, and R^2 are shown in *H*.

Discussion and Conclusion

We reported the presence of exogeneous fine particles in human CSF and blood, hinting at a potential transport of exogeneous fine particles from the bloodstream to the brain, which was confirmed mechanistically by in vitro and in vivo studies (Fig. 6). Kreyling (32) previously demonstrated that both the route from the lung via blood to the brain and the direct transport route via the olfactory nerves to the brain are responsible for the entry of NPs into the rat brain, with a higher accumulation mass (approximately eight times) observed to reach the brain through the nasal exposure route than through translocation to the bloodstream following exposure via the intratracheal inhalation route. Here, we further unraveled that the inhaled exogenous particles can enter the bloodstream after crossing the air–blood barrier and eventually, reach the brain, leading to damage of the BBB and surrounding tissues as they do so (Fig. 6). Furthermore, once they reached the brain, the particles were hard to clear from the brain and were retained for longer than in other organs.

Together, the data presented in this study thus support a link between environmental and occupational inhalation exposure and the presence of exogeneous fine particles in the brain, hinting at an important relationship between exogenous particle-induced neurotoxicity and brain disorders as previously suggested (14). These findings, hence, offer a line of evidence in proving the risks from particulate pollution to the CNS and in elucidating the exposure route of exogenous particles from inhalation to the brain. However, more direct proof of the exposure and transport pathways of ambient fine particles from inhalation via the bloodstream and damage of the BBB to the brain is needed, warranting further detailed investigation, including epidemiological studies, in the future. Nevertheless,

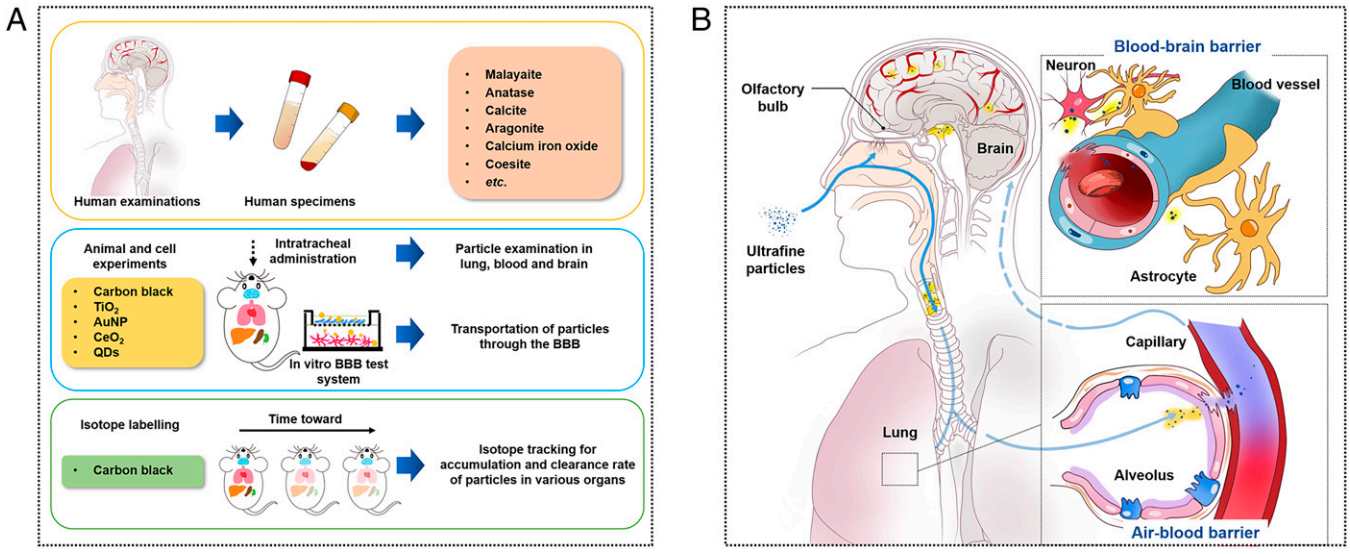

Fig. 6. A schematic diagram illustrating the integration of in vitro and in vivo approaches to explain the observations of exogenous fine particles in the CNS of human patients (*A*) and the plausible mechanisms underlying the passage of inhaled exogenous particles into the brain (*B*). The possible pathway is supported by the findings here, namely through inhalation into the brain tissue via blood circulation.

this work opens up an avenue via which to study the exposure and adverse effects of exogenous particles on the CNS under environmental and occupational settings.

Materials and Methods

Additional detailed information on materials and methods is provided in *SI Appendix*.

Human CSF and Blood Specimens. All human CSF and blood specimens were collected from patients with various brain disorders at the First Affiliated Hospital of Shandong First Medical University & Shandong Provincial Qianfoshan Hospital (Jinan, Shandong Province, China). All patients came from Shandong Province, China and had differential exposure scenarios based on their individual occupational and residential backgrounds. Human blood specimens for the healthy control individuals were collected from healthy young students and middle-aged and elderly employees at Shandong First Medical University & Shandong Academy of Medical Science. All participants provided informed consent. The study protocol was approved by the Medical Ethics Committee at the First Affiliated Hospital of Shandong First Medical University & Shandong Provincial Qianfoshan Hospital. All manipulations were carried out in accordance with the relevant guidelines and regulations.

Extraction and Purification of Exogenous Particles from Human CSF and Serum Specimens. The extraction and purification of exogenous particles from human CSF and serum specimens were implemented following a modified procedure as reported previously (25).

Characterization of Exogenous Particles in Human Specimens. The structure and elemental composition of exogenous particles were characterized on an HR-TEM (JEOL JEM-2010F; Hitachi) and an HAADF-STEM (JEOL JEM-ARM300F; Hitachi) with EDXS using an aberration-correction JEM-ARM300F operated at 300 kV.

Characterization of Experimental Exogenous Particles in Animal Studies. Details of the manufacturers, the synthesis procedures, and the related characterization are described in *SI Appendix*.

BBB Model Setup and the Particle Transport Experiments. The BBB model was established as described previously (30, 63). For the particle transport experiments, the transported particles were examined through HR-TEM (JEOL JEM-2010F; Hitachi) and ICP-MS (7500a; Agilent Technologies).

Synthesis and Characterization of ^{125}I-Labeled CB Particles. The labeling of CB particles with ^{125}I was performed following a modified protocol as reported previously (64). The stability of the labeled particles was assessed in PBS with or without 10% fetal bovine serum and analyzed by thin-layer chromatography.

Animal Experimentation. BALB/c mice (females, 6 to 7 wk old) were obtained from Vital River Laboratory Animal Technology Co. Ltd. All animal experimental protocols were approved by the Animal Ethics Committee at the Research Center for Eco-Environmental Sciences, Chinese Academy of Sciences (Beijing, China).

Data Availability. All study data are included in the article and/or *SI Appendix*.

ACKNOWLEDGMENTS. This project was supported by National Natural Science Foundation of China Grants 91943301, 21906175, 22150006, 21920102007, and 22021003; Beijing Natural Science Foundation Grant 8191002; and Shandong Province Natural Science Foundation Grant ZR202010300086. We thank Jing Xia for assistance with particle characterizations with an HAADF-STEM at the Technical Institute of Physics and Chemistry, Chinese Academy of Sciences, Beijing, China and Can Peng and Zhongshuang Lv for assistance with making mouse brain samples and characterizations through the Tecnai Spirit transmission electron microscopy at the Center for Biological Imaging, Institution of Biophysics, Chinese Academy of Sciences, Beijing, China. I.L. acknowledges funding from European Commission Horizon 2020 Funding Progamme Grants 814572 (NanoSolveIT), 814425 (RiskGone), and 731032 (NanoCommons).

Author affiliations: [a]State Key Laboratory of Environmental Chemistry and Ecotoxicology, Research Center for Eco-Environmental Sciences, Chinese Academy of Sciences, Beijing 100085, China; [b]College of Resources and Environment, University of Chinese Academy of Sciences, Beijing 100049, China; [c]Department of Neurosurgery, First Affiliated Hospital of Shandong First Medical University & Shandong Provincial Qianfoshan Hospital, Jinan 250014, China; [d]Department of Imaging, Jiangsu Huajing Molecular Imaging & Drug Research Institutes Co., Ltd., Changshu 215500, China; [e]Beijing Jishuitan Hospital, Peking University Health Science Center, Beijing Research Institute of Traumatology and Orthopaedics, Beijing 100035, China; [f]Science and Technology Innovation Center, Shandong First Medical University & Shandong Academy of Medical Sciences, Jinan 250000, China; and [g]School of Geography, Earth and Environmental Sciences, University of Birmingham, Birmingham B15 2TT, United Kingdom

1. J. Lelieveld, U. Pöschl, Chemists can help to solve the air-pollution health crisis. *Nature* **551**, 291–293 (2017).
2. P. J. Landrigan *et al.*, The Lancet Commission on pollution and health. *Lancet* **391**, 462–512 (2018).
3. A. J. Cohen *et al.*, Estimates and 25-year trends of the global burden of disease attributable to ambient air pollution: An analysis of data from the Global Burden of Diseases Study 2015. *Lancet* **389**, 1907–1918 (2017).
4. E. Underwood, The polluted brain. *Science* **355**, 342–345 (2017).
5. L. Peeples, News feature: How air pollution threatens brain health. *Proc. Natl. Acad. Sci. U.S.A.* **117**, 13856–13860 (2020).
6. L. Calderón-Garcidueñas *et al.*, Air pollution, cognitive deficits and brain abnormalities: A pilot study with children and dogs. *Brain Cogn.* **68**, 117–127 (2008).
7. L. Calderón-Garcidueñas *et al.*, Exposure to severe urban air pollution influences cognitive outcomes, brain volume and systemic inflammation in clinically healthy children. *Brain Cogn.* **77**, 345–355 (2011).
8. J. T. Jørgensen *et al.*, Long-term exposure to ambient air pollution and incidence of brain tumours: The Danish Nurse Cohort. *Neurotoxicology* **55**, 122–130 (2016).
9. M. Cacciottolo *et al.*, Particulate air pollutants, APOE alleles and their contributions to cognitive impairment in older women and to amyloidogenesis in experimental models. *Transl. Psychiatry* **7**, e1022 (2017).
10. Y. C. Chang, T. B. Cole, L. G. Costa, Prenatal and early-life diesel exhaust exposure causes autism-like behavioral changes in mice. *Part. Fibre Toxicol.* **15**, 18–32 (2018).
11. X. Zhang, X. Chen, X. Zhang, The impact of exposure to air pollution on cognitive performance. *Proc. Natl. Acad. Sci. U.S.A.* **115**, 9193–9197 (2018).
12. L. Calderón-Garcidueñas *et al.*, Hallmarks of Alzheimer disease are evolving relentlessly in Metropolitan Mexico City infants, children and young adults. APOE4 carriers have higher suicide risk and higher odds of reaching NFT stage V at ≤ 40 years of age. *Environ. Res.* **164**, 475–487 (2018).
13. B. A. Maher *et al.*, Magnetite pollution nanoparticles in the human brain. *Proc. Natl. Acad. Sci. U.S.A.* **113**, 10797–10801 (2016).
14. L. Calderón-Garcidueñas *et al.*, Quadruple abnormal protein aggregates in brainstem pathology and exogenous metal-rich magnetic nanoparticles (and engineered Ti-rich nanorods). The substantia nigrae is a very early target in young urbanites and the gastrointestinal tract a key brainstem portal. *Environ. Res.* **191**, 110139 (2020).
15. L. Calderón-Garcidueñas *et al.*, Air pollution and brain damage. *Toxicol. Pathol.* **30**, 373–389 (2002).
16. L. Calderón-Garcidueñas *et al.*, DNA damage in nasal and brain tissues of canines exposed to air pollutants is associated with evidence of chronic brain inflammation and neurodegeneration. *Toxicol. Pathol.* **31**, 524–538 (2003).
17. B. C. Nephew *et al.*, Traffic-related particulate matter affects behavior, inflammation, and neural integrity in a developmental rodent model. *Environ. Res.* **183**, 109242 (2020).
18. Y. C. Chang, R. Daza, R. Hevner, L. G. Costa, T. B. Cole, Prenatal and early life diesel exhaust exposure disrupts cortical lamina organization: Evidence for a reelin-related pathogenic pathway induced by interleukin-6. *Brain Behav. Immun.* **78**, 105–115 (2019).
19. Q. Ma, Y. Qi, Q. Shan, S. Liu, H. He, Understanding the knowledge gaps between air pollution controls and health impacts including pathogen epidemic. *Environ. Res.* **189**, 109949 (2020).
20. W. G. Kreyling *et al.*, Size dependence of the translocation of inhaled iridium and carbon nanoparticle aggregates from the lung of rats to the blood and secondary target organs. *Inhal. Toxicol.* **21** (suppl. 1), 55–60 (2009).
21. G. Oberdörster *et al.*, Extrapulmonary translocation of ultrafine carbon particles following whole-body inhalation exposure of rats. *J. Toxicol. Environ. Health A* **65**, 1531–1543 (2002).
22. G. Oberdörster *et al.*, Translocation of inhaled ultrafine particles to the brain. *Inhal. Toxicol.* **16**, 437–445 (2004).
23. M. Guttenberg *et al.*, Biodistribution of inhaled metal oxide nanoparticles mimicking occupational exposure: A preliminary investigation using enhanced darkfield microscopy. *J. Biophotonics* **9**, 987–993 (2016).
24. D. Li *et al.*, Fluorescent reconstitution on deposition of $PM_{2.5}$ in lung and extrapulmonary organs. *Proc. Natl. Acad. Sci. U.S.A.* **116**, 2488–2493 (2019).
25. D. Lu *et al.*, Chemical multi-fingerprinting of exogenous ultrafine particles in human serum and pleural effusion. *Nat. Commun.* **11**, 2567–2574 (2020).
26. L. Calderón-Garcidueñas *et al.*, Combustion- and friction-derived magnetic air pollution nanoparticles in human hearts. *Environ. Res.* **176**, 108567 (2019).
27. M. R. Miller *et al.*, Inhaled nanoparticles accumulate at sites of vascular disease. *ACS Nano* **11**, 4542–4552 (2017).
28. H. Bové *et al.*, Ambient black carbon particles reach the fetal side of human placenta. *Nat. Commun.* **10**, 3866–3873 (2019).
29. B. Obermeier, A. Verma, R. M. Ransohoff, The blood-brain barrier. *Handb. Clin. Neurol.* **133**, 39–59 (2016).
30. Z. Guo *et al.*, Biotransformation modulates the penetration of metallic nanomaterials across an artificial blood-brain barrier model. *Proc. Natl. Acad. Sci. U.S.A.* **118**, e2105245118 (2021).
31. A. Elder *et al.*, Translocation of inhaled ultrafine manganese oxide particles to the central nervous system. *Environ. Health Perspect.* **114**, 1172–1178 (2006).
32. W. G. Kreyling, Discovery of unique and ENM- specific pathophysiologic pathways: Comparison of the translocation of inhaled iridium nanoparticles from nasal epithelium versus alveolar epithelium towards the brain of rats. *Toxicol. Appl. Pharmacol.* **299**, 41–46 (2016).

33. R. M. Koffie *et al.*, Nanoparticles enhance brain delivery of blood-brain barrier-impermeable probes for in vivo optical and magnetic resonance imaging. *Proc. Natl. Acad. Sci. U.S.A.* **108**, 18837–18842 (2011).
34. G. R. Topal *et al.*, ApoE-targeting increases the transfer of solid lipid nanoparticles with donepezil cargo across a culture model of the blood-brain barrier. *Pharmaceutics* **13**, 38 (2020).
35. C. Pan *et al.*, Diagnostic values of cerebrospinal fluid t-tau and Aβ42 using Meso Scale Discovery assays for Alzheimer's disease. *J. Alzheimers Dis.* **45**, 709–719 (2015).
36. A. Montagne *et al.*, *APOE4* leads to blood-brain barrier dysfunction predicting cognitive decline. *Nature* **581**, 71–76 (2020).
37. D. van de Beek *et al.*, Clinical features and prognostic factors in adults with bacterial meningitis. *N. Engl. J. Med.* **351**, 1849–1859 (2004).
38. K. Greisen, M. Loeffelholz, A. Purohit, D. Leong, PCR primers and probes for the 16S rRNA gene of most species of pathogenic bacteria, including bacteria found in cerebrospinal fluid. *J. Clin. Microbiol.* **32**, 335–351 (1994).
39. R. Bonewitz, *Rocks and Minerals* (DK Publishing, London, United Kingdom, ed. 2, 2012).
40. K. R. Daellenbach *et al.*, Sources of particulate-matter air pollution and its oxidative potential in Europe. *Nature* **587**, 414–419 (2020).
41. Y. C. Lin *et al.*, Chemical characterization of $PM_{2.5}$ emissions and atmospheric metallic element concentrations in $PM_{2.5}$ emitted from mobile source gasoline-fueled vehicles. *Sci. Total Environ.* **739**, 139942 (2020).
42. E. E. Feld-Cook, L. Bovenkamp-Langlois, S. M. Lomnicki, Effect of particulate matter mineral composition on environmentally persistent free radical (EPFR) formation. *Environ. Sci. Technol.* **51**, 10396–10402 (2017).
43. Y. Qi *et al.*, Intrusion of inhaled exotic ultrafine particles into the knee joint in humans and animals: A risk to the joint and surrounding tissues. *Nano Today* **43**, 101426 (2022).
44. J. B. Higgins, P. H. Ribbe, The structure of malayaite, $CaSnOSiO_4$, a tin analog of titanite. *Am. Mineral.* **62**, 801–806 (1977).
45. X. Chen, S. S. Mao, Titanium dioxide nanomaterials: Synthesis, properties, modifications, and applications. *Chem. Rev.* **107**, 2891–2959 (2007).
46. S. M. Aleksandrov, M. A. Troneva, Composition, mineral assemblages, and genesis of titanite and malayaite in skarns. *Geochem. Int.* **45**, 1012–1024 (2007).
47. Z. Le, Z. Pi, C. Yang, X. Tian, S. Zhang, Synthesis of chromium-doped malayaite pigments from wastewater containing low chromium(VI). *J. Air Waste Manag. Assoc.* **60**, 1257–1261 (2010).
48. M. Shakeel *et al.*, Toxicity of nano-titanium dioxide (TiO_2-NP) through various routes of exposure: A review. *Biol. Trace Elem. Res.* **172**, 1–36 (2016).
49. W. G. Kreyling *et al.*, Quantitative biokinetics over a 28 day period of freshly generated, pristine, 20 nm titanium dioxide nanoparticle aerosols in healthy adult rats after a single two-hour inhalation exposure. *Part. Fibre Toxicol.* **16**, 29–56 (2019).
50. C. Tigchelaar *et al.*, The Anaesthetic Biobank of Cerebrospinal fluid: A unique repository for neuroscientific biomarker research. *Ann. Transl. Med.* **9**, 455 (2021).
51. I. Lynch *et al.*, The bio-nano-interface in predicting nanoparticle fate and behaviour in living organisms: Towards grouping and categorising nanomaterials and ensuring nanosafety by design. *BioNanoMaterials* **14**, 195–216 (2013).
52. J. Tang *et al.*, Distribution, translocation and accumulation of silver nanoparticles in rats. *J. Nanosci. Nanotechnol.* **9**, 4924–4932 (2009).
53. J. Tang *et al.*, Silver nanoparticles crossing through and distribution in the blood-brain barrier in vitro. *J. Nanosci. Nanotechnol.* **10**, 6313–6317 (2010).
54. B. A. Maher, A. González-Maciel, R. Reynoso-Robles, R. Torres-Jardón, L. Calderón-Garcidueñas, Iron-rich air pollution nanoparticles: An unrecognised environmental risk factor for myocardial mitochondrial dysfunction and cardiac oxidative stress. *Environ. Res.* **188**, 109816 (2020).
55. N. M. Liu *et al.*, Evidence for the presence of air pollution nanoparticles in placental tissue cells. *Sci. Total Environ.* **751**, 142235 (2021).
56. H. Chen, C. E. Nanayakkara, V. H. Grassian, Titanium dioxide photocatalysis in atmospheric chemistry. *Chem. Rev.* **112**, 5919–5948 (2012).
57. M. Mei *et al.*, Early-life exposure to three size-fractionated ultrafine and fine atmospheric particulates in Beijing exacerbates asthma development in mature mice. *Part. Fibre Toxicol.* **15**, 13 (2018).
58. P. H. Danielsen *et al.*, Nanomaterial- and shape-dependency of TLR2 and TLR4 mediated signaling following pulmonary exposure to carbonaceous nanomaterials in mice. *Part. Fibre Toxicol.* **18**, 40 (2021).
59. X. Liu *et al.*, Serum apolipoprotein A-I depletion is causative to silica nanoparticles-induced cardiovascular damage. *Proc. Natl. Acad. Sci. U.S.A.* **118**,e2108131118 (2021).
60. Y. Morimoto *et al.*, Comparison of pulmonary inflammatory responses following intratracheal instillation and inhalation of nanoparticles. *Nanotoxicology* **10**, 607–618 (2016).
61. R. M. Silva *et al.*, Instillation versus inhalation of multiwalled carbon nanotubes: Exposure-related health effects, clearance, and the role of particle characteristics. *ACS Nano* **8**, 8911–8931 (2014).
62. Y. Lin *et al.*, Rapid, solventless, bulk preparation of metal nanoparticle-decorated carbon nanotubes. *ACS Nano* **3**, 871–884 (2009).
63. S. Nakagawa *et al.*, A new blood-brain barrier model using primary rat brain endothelial cells, pericytes and astrocytes. *Neurochem. Int.* **54**, 253–263 (2009).
64. K. Yang *et al.*, *In vivo* pharmacokinetics, long-term biodistribution, and toxicology of PEGylated graphene in mice. *ACS Nano* **5**, 516–522 (2011).
65. X. Zhang *et al.*, Distribution and biocompatibility studies of graphene oxide in mice after intravenous administration. *Carbon* **49**, 986–995 (2011).
66. J. K. Kim *et al.*, Lung retention and particokinetics of silver and gold nanoparticles in rats following subacute inhalation co-exposure. *Part. Fibre Toxicol.* **18**, 5–17 (2021).
67. A. D. Wong *et al.*, The blood-brain barrier: An engineering perspective. *Front. Neuroeng.* **6**, 7 (2013).
68. D. Polikarpov *et al.*, Mossbauer evidence of $^{57}Fe_3O_4$ based ferrofluid biodegradation in the brain. *Hyperfine Interact.* **226**, 421–430 (2014).